# Virtual Suspension Control in Two-Wheeled Robot

1st Makoto Mezawa
*Graduate School of Integrated Design Engineering, Keio University*
Yokohama, Japan
mezawa@sum.sd.keio.ac.jp

2nd Toshiyuki Murakami
*Department of System Design Engineering, Keio University*
Yokohama, Japan
mura@sd.keio.ac.jp

***Abstract*—Two-wheeled robots are expected to work together with humans. This paper addresses a two-wheeled robot with an arm that can retrieve things from shelves. When the robot is moved, there is a possibility that the shape of the wheels and the road surface condition may cause damage to the load. To improve this drawback, this paper proposes the application of compliance control to the arm. To prevent the arm from continuously tilting, the DC component was removed from the force applied to the arm by a high-pass filter. The effectiveness of the proposed method is confirmed through experiments. From the results obtained, it is confirmed that the proposed method reduces the peak value of the angular acceleration of the load and thereby improves the tracking performance.**

***Index Terms*—Two-wheeled robot, Wheeled inverted pendulum, Virtual suspension control, Compliance control**

## I. Introduction

In recent years, labor shortages due to the declining birthrate and aging population have become a major social issue. To compensate for the shortage of labor, it will be necessary for humans and robots to work together. Humans have a small footprint and a high center of gravity (CoG), and workspaces are designed for these human characteristics. To adapt to such environment, robots that work with humans should be designed to possess these characteristics of humans. A two-wheeled robot (TWR) is a mechanism with the features of a small footprint and high CoG.

TWR has actuators on both the left and right wheels. In addition, TWR has three degrees of freedom together in position and posture, making it an underactuated system. Since TWR is statically unstable, the posture must be stabilized by controlling the wheel motors.

Much research and development has been done on two-wheeled robots [1]. F. Grasser et al. performed linearized approximation in the neighborhood of the inverted state, which is the equilibrium point, and achieved posture stabilization using the pole placement method [2]. K. Pathak et al. derived a new model by performing partial linearized feedback and used it for posture stabilization [3]. Nakamura et al. developed a pitch angle disturbance observer (PADO) that estimates and compensates for pitch angle disturbances of a wheelchair and determines control inputs based on Lyapunov's stability theorem to achieve posture stabilization of a wheelchair-type two-wheel robot [4]. Hirata developed a synthesized pitch angle disturbance observer (SPADO) that collectively compensates for pitch angle disturbance and wheel disturbance [5]. Acar et al. proposed gravity compensation with repulsive compliance control (RCC) to deal with human CoG fluctuations in a wheelchair [6]; RCC dynamically generates a pitch angle command value in the direction that opposes the disturbance applied to the pitch angle according to a set impedance characteristic, thereby this method suppresses the movement of the CoG. In a study of placing objects on a TWR, Sayidmarie analyzed the effect that the height of the CoG of the object to be transported has on the stability of the robot [7], and Takei et al. proposed a method for re-setting the CoG when a load is placed on the TWR, using the fact that the CoG is directly above the axle when the TWR is stationary [8]. In a study of a two-wheeled robot with arms, Yajima et al. adapted RCC to a TWR to compensate for changes in the CoG of the vehicle [9].

Previous studies have not considered the effects of disturbance on the load. The shape of the wheels and the unevenness of the ground may cause the arm to vibrate or shake when the TWR moves. Vibration and shaking can cause crushing, rubbing, and denting of the load. In addition, when vibration and shaking are large, there is a risk of damage to the load. Therefore, it is necessary to prevent vibrations and shaking from being transmitted to the load.

This paper proposes a control method to suppress the influence of the load by moving the arm along the disturbance. Compliance control is used to control a robot's arm so that it move in response to a force. Compliance control has been studied widely and is particularly effective in human cooperation [10]. Sadeghian et al. used manipulator redundancy to control compliance, allowing it to cope with human interference [11]. Ugurlu et al. deal with external forces generated during walking by incorporating active compliance in a lower limb exoskeleton robot [12]. The reaction torque observer (RTOB) introduced into the arm motor is used to estimate the torque applied to the arm, and this value is used as input for compliance control [13]. However, if the RTOB value is used as input as is, the arm will remain tilted by the gravity of the luggage. If the arm remains tilted, the load will fall and cannot be used to hold the object. To address this problem, a high-pass filter is used to remove the DC component from the force applied to the arm.

This paper is organized as follows: In section II, the modeling of the TWR is described. In Section III, the control system of the TWR is explained. In section IV, the validity of

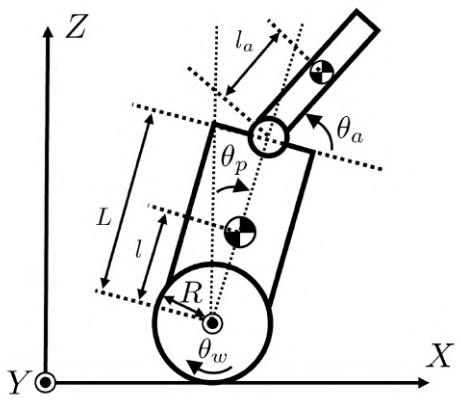


Fig. 1. Side view of two-wheeled robot with an arm

TABLE I
NOTATIONS ABOUT TWO-WHEELED ROBOT WITH AN ARM

| Notation | Explanation |
|---|---|
| $R$ | Radius of wheels |
| $l$ | Distance between wheel motor axle and the CoG of body |
| $L$ | Height of body |
| $l_a$ | Distance between arm motor axle and the CoG of arm |
| $\theta_w$ | Rotation angle of wheels |
| $\theta_p$ | Pitch angle of body |
| $\theta_a$ | Angle of arm |
| $x$ | Wheel position |
| $n_w$ | Gear ratio of wheel motor torque |
| $n_a$ | Gear ratio of arm motor torque |
| $\tau_w$ | Wheel motor torque |
| $\tau_a$ | Arm motor torque |

the proposed method is evaluated through experiments. Finally, section V describes the conclusion.

## II. MODELING

This section describes the dynamics of the TWR. Since this paper does not consider turning, we consider model in the XZ plane. The side view of the TWR with an arm as shown in Fig. 1. Notations about Fig. 1 are listed in Table I.

$x$ and $\theta_w$ are related by (1). It is assumed that the wheel does not slip.

$$\dot{x} = R\dot{\theta}_w \tag{1}$$

The equation of motion for TWR with an arm becomes (2) by using the Lagrangian method.

$$\boldsymbol{M}(\boldsymbol{\theta})\ddot{\boldsymbol{\theta}} + \boldsymbol{H}(\boldsymbol{\theta}, \dot{\boldsymbol{\theta}}) + \boldsymbol{G}(\boldsymbol{\theta}) = \boldsymbol{E}\boldsymbol{\tau} \tag{2}$$

$\boldsymbol{M}$ is the inertia matrix, $\boldsymbol{H}$ is the centrifugal and Coriolis forces, $\boldsymbol{G}$ is the term representing the gravity load, and $\boldsymbol{E}\boldsymbol{\tau}$ is the generalized force, respectively. The structure of each matrix is shown from (3) to (7).

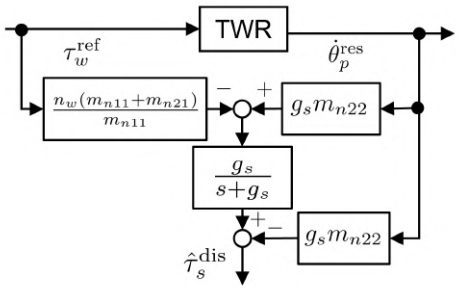


Fig. 2. Block diagram of SPADO

$$\boldsymbol{\theta} = \begin{bmatrix}\theta_w & \theta_p & \theta_a\end{bmatrix}^{\mathrm{T}} \tag{3}$$

$$\boldsymbol{M}(\theta) = \begin{bmatrix} m_{11} & m_{12} & m_{13} \\ m_{21} & m_{22} & m_{23} \\ m_{31} & m_{32} & m_{33} \end{bmatrix} \tag{4}$$

$$\boldsymbol{H} = \begin{bmatrix}h_1 & h_2 & h_3\end{bmatrix}^{\mathrm{T}} \tag{5}$$

$$\boldsymbol{G} = \begin{bmatrix}0 & g_2 & g_3\end{bmatrix}^{\mathrm{T}} \tag{6}$$

$$\boldsymbol{E}\boldsymbol{\tau} = \begin{bmatrix}n_w\tau_w & -n_w\tau_w & n_a\tau_a\end{bmatrix}^{\mathrm{T}} \tag{7}$$

## III. CONTROL SYSTEM DESIGN

In this section, control system is considered. The body has a synthesized pitch angle disturbance observer (SPADO) and a repulsive compliance control (RCC) for CoG deviation compensation. The body also has tracking and attitude stabilization control based on the Lyapunov stability theorem. The arm have DOB and RTOB, and the compliance control is based on the RTOB results. The arm use the results of the observer to generate angle commands. Each of the control systems is described below.

### A. Synthesized pitch angle disturbance observer (SPADO)

To estimate the disturbance affecting the pitch angle and wheel angle of a TWR, a synthesized pitch angle disturbance observer (SPADO) is designed on the vehicle body. Block diagram is shown in Fig. 2.

The equations of motion for the wheel rotation angle $\theta_w$ and the pitch angle $\theta_p$ become (8) and (9) respectively. $\tilde{\tau}_w^{\mathrm{dis}}$ and $\tilde{\tau}_p^{\mathrm{dis}}$ are the total disturbances, including the disturbance term, the internal interference force, the gravity term, and the inertial variation, which are expressed by (10) and (11), respectively.

$$m_{n11}\ddot{\theta}_w^{\mathrm{res}} = n_w\tau_w^{\mathrm{ref}} - \tilde{\tau}_w^{\mathrm{dis}} \tag{8}$$

$$m_{n21}\ddot{\theta}_w^{\mathrm{res}} + m_{n22}\ddot{\theta}_p^{\mathrm{res}} = -n_w\tau_w^{\mathrm{ref}} - \tilde{\tau}_p^{\mathrm{dis}} \tag{9}$$

$$\tilde{\tau}_w^{\mathrm{dis}} = m_{12}\ddot{\theta}_p^{\mathrm{res}} + m_{13}\ddot{\theta}_a^{\mathrm{res}} + (m_{11} - m_{n11})\ddot{\theta}_w^{\mathrm{res}} + h_1 + T_{lw} \tag{10}$$

$$\tilde{\tau}_p^{\mathrm{dis}} = m_{23}\ddot{\theta}_a^{\mathrm{res}} + (m_{21} - m_{n21})\ddot{\theta}_w^{\mathrm{res}} + (m_{22} - m_{n22})\ddot{\theta}_p^{\mathrm{res}} + h_2 + g_2 + T_{lp} \tag{11}$$

The subscript $n$ is the nominal value of each matrix component in (4).

$T_{lw}$ and $T_{lp}$ represent the disturbance term including external forces and friction. (9) can be transformed into (12) by substituting (8).

$$m_{n22}\ddot{\theta}_p^{\mathrm{res}} + \frac{m_{n21}+m_{n11}}{m_{n11}} n_w \tau_w^{\mathrm{ref}} = -\tilde{\tau}_s^{\mathrm{dis}} \tag{12}$$

$$\tilde{\tau}_s^{\mathrm{dis}} = \tilde{\tau}_p^{\mathrm{dis}} - \frac{m_{n21}}{m_{n11}} \tilde{\tau}_w^{\mathrm{dis}} \tag{13}$$

To suppress the amplification of high-frequency noise due to differentiation, a pseudo-differentiation using a first-order low-pass filter (LPF) is used to obtain an estimate of the disturbance $\hat{\tau}_s^{\mathrm{dis}}$ using (14).

$$\hat{\tau}_s^{\mathrm{dis}} = -\frac{g_s}{s+g_s}\left(\frac{m_{n21}+m_{n11}}{m_{n11}} n_w \tau_w^{\mathrm{ref}} - g_s m_{n22}\dot{\theta}_p^{\mathrm{res}}\right) - g_s m_{n22}\dot{\theta}_p^{\mathrm{res}} \tag{14}$$

$g_s$ is the cutoff frequency of LPF.

### B. Repulsive Compliance Control (RCC)

RCC generates a pitch angle command value for CoG position deviation compensation. When a load is placed on the robot, a change in the CoG of the system causes a disturbance in the pitch angle direction, which causes the robot to constantly accelerate. By applying RCC, the pitch angle converges to an angle that compensates for the CoG position deviation, thereby suppressing the acceleration of the robot due to CoG position deviation.

The impedance model in RCC is shown in (15).

$$M_{rcc}\ddot{\theta}_{pc}^{\mathrm{cmd}} + D_{rcc}\dot{\theta}_{pc}^{\mathrm{cmd}} + K_{rcc}\theta_{pc}^{\mathrm{cmd}} = -A_{rcc}\hat{\tau}_a^{\mathrm{ext}} \tag{15}$$

$M_{rcc}$, $D_{rcc}$, and $K_{rcc}$ are the virtual inertia, viscosity, and stiffness coefficients, respectively, while $A_{rcc}$ is the external force assist gain. The input is $\hat{\tau}_a^{\mathrm{ext}}$, obtained from the RTOB.

### C. Wheel position control

In this research, wheel position control is constructed outside of posture stabilization control. The wheel position control consists of a PI controller and a phase compensator. The phase compensator is used to remove unstable poles that cause pitch angle oscillations. The pitch angle command value $\theta_p^{\mathrm{cmd}}$ is shown by (16).

$$\theta_p^{\mathrm{cmd}} = K_{pw}(\theta_w^{\mathrm{cmd}} - \theta_w^{\mathrm{res}}) + K_{iw}\int(\theta_w^{\mathrm{cmd}} - \theta_w^{\mathrm{res}})dt + \theta_{pc}^{\mathrm{cmd}} \tag{16}$$

$K_{pw}$, $K_{iw}$ are propotional gain and integral gain.

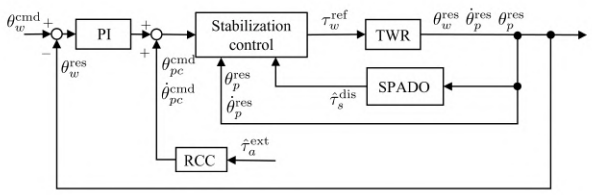


Fig. 3. Block diagram of the entire control system in the body section

### D. Lyapunov based posture stabilization control

A TWR is an unstable system in the pitch angle direction, and posture stabilization control is necessary to maintain the inverted state. System stabilization is achieved by determining the torque reference values of the wheels based on the Lyapunov stability theorem. First, the Lyapunov function $V$ is set as in (17).

$$V = \frac{1}{2}K_1(\theta_p^{\mathrm{cmd}} - \theta_p^{\mathrm{res}})^2 + \frac{1}{2}K_2(\dot{\theta}_p^{\mathrm{cmd}} - \dot{\theta}_p^{\mathrm{res}})^2 \tag{17}$$

$K_1$, $K_2$ are positive gain. The derivative of $V$ is shown in (18), by substituting (12).

$$\dot{V} = (\dot{\theta}_p^{\mathrm{cmd}} - \dot{\theta}_p^{\mathrm{res}})\left[K_1(\theta_p^{\mathrm{cmd}} - \theta_p^{\mathrm{res}}) + K_2\left\{\ddot{\theta}_p^{\mathrm{cmd}} + \frac{1}{m_{n22}}\left(\frac{n_w(m_{n21}+m_{n11})}{m'_{n11}}\tau_w^{\mathrm{ref}} + \tilde{\tau}_s^{\mathrm{dis}}\right)\right\}\right] \tag{18}$$

If $V$ is of the form in (19), $\dot{V}$ is semi-negative and $\dot{V}$ is zero only at the equilibrium point, thus guaranteeing the stability of the system by LaSalle's theorem.

$$\dot{V} = -K_3(\dot{\theta}_p^{\mathrm{cmd}} - \dot{\theta}_p^{\mathrm{res}})^2 \tag{19}$$

$K_3$ is a positive gain. Comparing (18) and (19), stability can be guaranteed by setting the wheel torque reference value $\tau_w^{\mathrm{cmd}}$ to (20).

$$\tau_w^{\mathrm{cmd}} = -\frac{m_{n11}m_{n22}}{n_w(m_{n21}+m_{n11})}\left\{\frac{K_1}{K_2}(\theta_p^{\mathrm{cmd}} - \theta_p^{\mathrm{res}}) + \frac{K_3}{K_2}(\dot{\theta}_p^{\mathrm{cmd}} - \dot{\theta}_p^{\mathrm{res}}) + \ddot{\theta}_p^{\mathrm{cmd}}\right\} - \frac{m_{n11}}{n_w(m_{n21}+m_{n11})}\tilde{\tau}_s^{\mathrm{dis}} \tag{20}$$

Fig. 3 shows a block diagram of the entire control system in the body section.

### E. Arm Angle Disturbance Observer

This section describes the design of an observer to estimate the disturbance affecting the arm angle $\theta_a$. The equation of motion for the arm angle is given by (21). $\tilde{\tau}_a^{\mathrm{dis}}$ is the total disturbance that summarizes the disturbance term, internal interfering forces, gravity term, and inertial variations.

$$m_{n33}\ddot{\theta}_a^{\mathrm{res}} = n_a\tau_a^{\mathrm{ref}} - \tilde{\tau}_a^{\mathrm{dis}} \tag{21}$$

To suppress the amplification of high-frequency noise due to differentiation, a pseudo-differentiation using a first-order LPF is used to obtain an estimate of the disturbance $\hat{\tau}_a^{\mathrm{dis}}$ using (22).

$$\hat{\tau}_a^{\mathrm{dis}} = \frac{g_a}{s+g_a}\left(n_a\tau_a^{\mathrm{ref}} + g_a m_{n33}\dot{\theta}_a^{\mathrm{res}}\right) - g_a m_{n33}\dot{\theta}_a^{\mathrm{res}} \quad (22)$$

$g_a$ is the cutoff frequency of LPF.

### F. Reaction Torque Observer (RTOB)

This section describes RTOB, which is used as an input for RCC and compliance control to estimate the reaction torque received by the arm without using a force or torque sensor. Reaction torque can be estimated as (23) and can be transformed as (24) by using pseudo differentiation.

$$\tau_a^{\mathrm{ext}} = n_a\tau_a^{\mathrm{ref}} - m_{n33}\ddot{\theta}_a^{\mathrm{res}} - g_3 - \tau_a^{\mathrm{fric}} \quad (23)$$

$$\hat{\tau}_a^{\mathrm{ext}} = \frac{g_{ra}}{s+g_{ra}}\left(n_a\tau_a^{\mathrm{ref}} + g_{ra}m'_{n33}\dot{\theta}_a^{\mathrm{res}} - g_3 - \tau_a^{\mathrm{fric}}\right) - g_{ra}m_{n33}\dot{\theta}_a^{\mathrm{res}} \quad (24)$$

$\tau_a^{\mathrm{fric}}$ is the frictional torque of the arm. $g_{ra}$ is the cutoff frequency of LPF.

### G. Compliance Control for Arm

Compliance control is applied to mitigate the impact of the load by moving the arm by the forces received from the TWR. The arm must not remain tilted in line with the weight of the object to prevent the object from falling. The input to the compliance control requires the reduction of the DC component from the forces applied to the arm. The DC component includes gravity due to the mass of the load. The input is shown as (7) by using a high pass filter.

$$\hat{\tau}_a^{'\mathrm{ext}} = \frac{s}{s+g_h}\hat{\tau}_a^{\mathrm{ext}} \quad (25)$$

$g_h$ is the cutoff frequency of high pass filter.

(26) shows a virtual impedance model for compliance control using the input $\hat{\tau}_a^{'ext}$ obtained by (25).

$$M_{cc}\ddot{\theta}_{ac}^{\mathrm{cmd}} + D_{cc}\dot{\theta}_{ac}^{\mathrm{cmd}} + K_{cc}\theta_{ac}^{\mathrm{cmd}} = A_{cc}\hat{\tau}_a^{'\mathrm{ext}} \quad (26)$$

$M_{cc}$, $D_{cc}$, and $K_{cc}$ represent the virtual inertia, viscosity, and stiffness coefficients, respectively. $A_{cc}$ represents the external force assist gain. (26) is used to generate the command values for arm angle $\theta_{ac}^{\mathrm{cmd}}$, angular velocity $\dot{\theta}_{ac}^{\mathrm{cmd}}$, and angular acceleration $\ddot{\theta}_{ac}^{\mathrm{cmd}}$. Fig. 4 shows a block diagram of the compliance control.

### H. Arm angle control

The arm must be horizontal to the ground for the material to be stable without falling. Considering the presence of disturbance, the arm angular command value becomes (27) using the value obtained by compliance control.

$$\theta_a^{\mathrm{cmd}} = \theta_p^{\mathrm{res}} - \theta_{ac}^{\mathrm{cmd}} \quad (27)$$

Since the arm angular velocity should be zero, the arm angular velocity command value becomes (28).

$$\dot{\theta}_a^{\mathrm{cmd}} = -\dot{\theta}_{ac}^{\mathrm{cmd}} \quad (28)$$

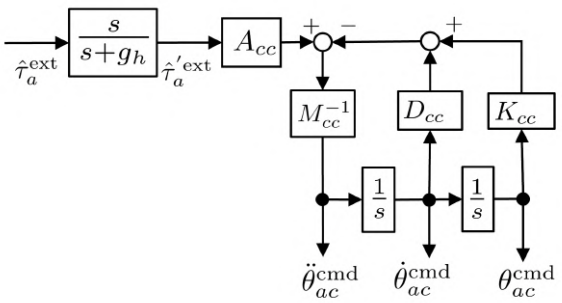


Fig. 4. Block diagram of compliance control

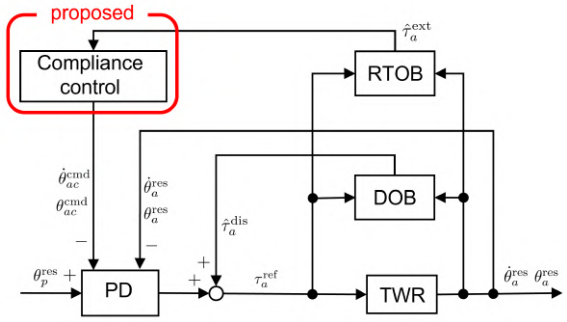


Fig. 5. Block diagram of the entire control system in the arm section

By performing PD control using the arm angular command values obtained from (27) and (28), and compensating for the arm angular disturbance, the arm torque reference value as the control input can be obtained from (29).

$$\tau_a^{\mathrm{ref}} = K_{pa}(\theta_a^{\mathrm{cmd}} - \theta_a^{\mathrm{res}}) + K_{da}(\dot{\theta}_a^{\mathrm{cmd}} - \dot{\theta}_a^{\mathrm{res}}) + \frac{\hat{\tau}_a^{\mathrm{dis}}}{n_a} \quad (29)$$

$K_{pa}$ and $K_{da}$ are proportional and differential gains, respectively. Fig. 5 shows a block diagram of the entire control system in the arm section.

## IV. Experiment

In this section, experiments are described. The proposed compliance control method applied to the arm was verified to be effective in reducing impact by using actual equipment.

To experiment under the assumption that the robot has uneven tires, a piece of plastic about 1 mm thick was attached at 5 cm intervals around the circumference of the wheel.

First, a two-wheeled robot was placed in an inverted position, and then an object was placed on the robot. To measure the angular acceleration of the object, a gyroscope sensor was included in the object. The vehicle was stopped in place for 12 seconds to reduce the effect of loading on the arm and the posture of the vehicle body. The vehicle was then moved forward 1.5 m at a speed of 0.25 m/s and a maximum acceleration of 0.25 m/s$^2$. The vehicle was stopped in place for 6 seconds and then moved backward 1.3 m at the same

TABLE II
PARAMETER USED IN EXPERIMENT

| Parameter | Explanation | Value |
|---|---|---|
| $K_{pw}$ | P-gain of wheel position control | 4.5 |
| $K_{iw}$ | I-gain of wheel position control | 0.6 |
| $\frac{K_1}{K_2}$ | P-gain of pitch angle control | 200 |
| $\frac{K_3}{K_2}$ | D-gain of pitch angle control | $20\sqrt{2}$ |
| $K_{pa}$ | P-gain of arm position control | 4.5 |
| $K_{da}$ | D-gain of arm position control | 4.5 |
| $g_s$ | Cutoff frequency of SPADO | 4 Hz |
| $M_{rcc}$ | Virtual mass of RCC | 0.137 |
| $D_{rcc}$ | Virtual damper of RCC | 1.549 |
| $K_{rcc}$ | Virtual spring of RCC | 4.381 |
| $A_{rcc}$ | Assist gain of RCC | 1.5 |
| $g_f$ | Cutoff frequency of FDOB | 5 Hz |
| $g_{rf}$ | Cutoff frequency of RTOB | 15 Hz |
| $M_{cc}$ | Virtual mass of compliance control | 0.04 |
| $D_{cc}$ | Virtual damper of compliance control | 0.24 |
| $K_{cc}$ | Virtual spring of compliance control | 0.36 |
| $A_{cc}$ | Assist gain of compliance control | 1.8 |
| $g_h$ | Cutoff frequency of highpass filter | 0.5 Hz |

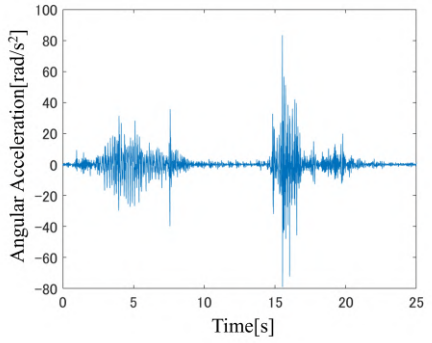


Fig. 6. Angular acceleration by the conventional method

speed and maximum acceleration as when moving forward. Table II shows the control parameters used in this experiment. The mass of the load was 3.74 kg, including the sensors.

Fig. 6 and Fig. 7 show the experimental results of angular acceleration by the conventional method and the proposed method, respectively. From the results, it can be seen that the peak acceleration of the angular acceleration has been reduced both in the forward and backward directions.

Fig. 8 and Fig. 9 show the pitch angle $\theta_p$, arm angle $\theta_a$, and their difference $\theta_{a-p}$ for the conventional and proposed methods, respectively. The difference between the pitch angle and the arm angle $\theta_{a-p}$ indicates the inclination of the arm relative to the ground.

From Fig. 8 and Fig. 9, it can be confirmed that the inverted state can be maintained even when the proposed method is used. Although the tilt of the arm relative to the ground increased with the proposed method compared to the conventional method, no problems that would interfere with holding an object, such as falling, were observed. Therefore, the proposed method does not affect the posture stabilization control that would interfere with object retention. Finally,

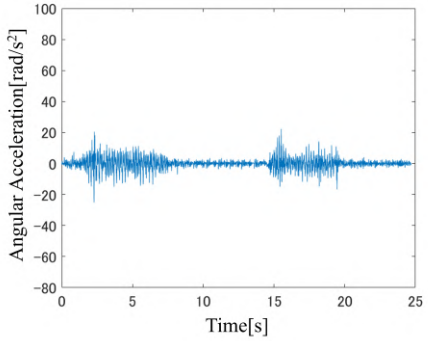


Fig. 7. Angular acceleration by the proposed method

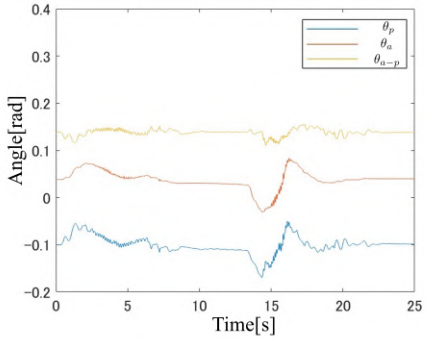


Fig. 8. Experimental result of posture by the conventional method

Fig. 10 and Fig. 11 show the trajectory responses of the conventional and proposed methods, respectively.

Fig. 10 and Fig. 11 show that the tracking performance of the proposed method is improved compared to the conventional method. There is a discrepancy between the command and response values at 0 seconds. The reason is as follows. The robot moved forward due to the effect of RCC when a load was placed. Next, even though the position controller has an integrator, it did not return after a certain time. It was

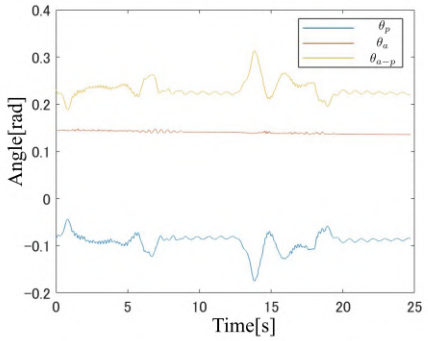


Fig. 9. Experimental result of posture by the proposed method

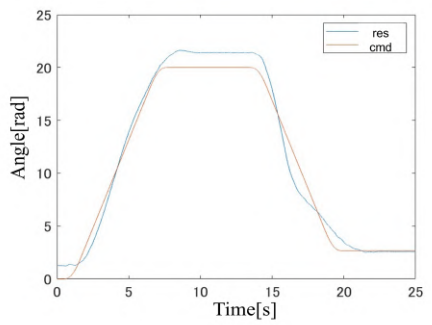


Fig. 10. Trajectory response by the conventional method

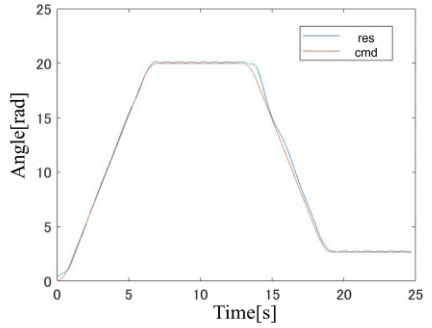


Fig. 11. Trajectory response by the proposed method

shown that the proposed method can move the robot more accurately according to the command values. This may be due to the improved tracking performance caused by the more stable posture of the proposed method.

## V. Conclusion

In this study, we proposed a virtual suspension control using compliance control to suppress the impact of a two-wheeled robot on an object. By using compliance control, the arm is controlled to follow the force, thereby suppressing the impact on the object. To prevent the arm from continuously tilting, a high-pass filter was used as the input for the compliance control to eliminate the DC component from the value output by RTOB. In this study, the effectiveness of the proposed method was verified through experiments. In the experiment, the peak value of the angular acceleration was reduced by the proposed method. This indicates that the effect of impact on the object was suppressed. Furthermore, the posture response results show that the proposed method does not affect the posture stabilization control of the two-wheeled robot. The trajectory response results indicate that the tracking control is further improved by the stabilization of the object by the proposed method.

## References

[1] Ronald Ping Man Chan, Karl A. Stol, C. Roger Halkyard, "Review of modelling and control of two-wheeled robots," Annual Reviews in Control, vol. 37, Issue 1, pp. 89-103, 2013.

[2] F. Grasser, A. D ' Arrigo, S. Colombi, and A. C. Rufer, "Joe: a mobile, inverted pendulum," IEEE Transactions on Industrial Electronics, Vol. 49, No. 1, pp. 107-114, 2002.

[3] K. Pathak, J. Franch, and S. K. Agrawal, "Velocity and position control of a wheeled inverted pendulum by partial feedback linearization," IEEE Transactions on Robotics, Vol. 21, No. 3, pp. 505-513, 2005.

[4] A. Nakamura, T. Murakami, "A Stabilization Control of Two Wheels Driven Wheelchair," 2009 IEEE/RSJ International Conference on Intelligent Robots and Systems, pp. 4863-4868, 2009.

[5] K. Hirata and T. Murakami, "A realization of step passage motion in two-wheel wheelchair systems utilizing variable repulsive compliance control," 2013 IEEE International Symposium on Industrial Electronics, Taipei, Taiwan, pp. 1-6, 2013.

[6] C. Acar, T. Murakami, "Center of Gravity Compensation for Dynamically-Balanced Two-Wheeled Wheelchair System", IEEJ Transactions on Industry Applications, Vol.131, No.5, pp.714-720, 2011.

[7] O. K. Sayidmarie, M. O. Tokhi, and S. A. Agouri, "Impact of dynamically moving payload on two wheeled robot stability," 19th International Conference on Methods and Models in Automation and Robotics (MMAR), pp. 915-920, 2014.

[8] T. Takei, R. Imamura, "Baggage Transportation and Navigation by a Wheeled Inverted Pendulum Mobile Robot," IEEE Transactions on Industrial electronics, Vol.56, No.10, pp.3985-3994, 2009.

[9] H. Yajima, K. Ishizaki, Y. Miyata, M. Nawa, N. Kato, and T. Murakami, "Posture Stabilization Control Compensating Variation of Body Center of Gravity in Underactuated System," 2023 IEEE International Conference on Mechatronics (ICM), Loughborough, UK, 2023.

[10] A. Calanca, R. Muradore, and P. Fiorini, "A review of algorithms for compliant control of stiff and fixed-compliance robots," IEEE/ASME Transactions on Mechatronics, Vol.21, No.2, pp.613-624, 2014.

[11] H. Sadeghian, L. Villani, M. Keshmiri, and B. Siciliano, "Task-Space Control of Robot Manipulators With Null-Space Compliance," IEEE Transactions on Robotics, Vol.30, No.2, pp.493-506, 2014.

[12] B. Ugurlu, H. Oshima, E. Sariyildiz, T. Narikiyo, and J. Babic, "Active Compliance Control Reduces Upper Body Effort in Exoskeleton-Supported Walking", IEEE Transactions on Human-Machine Systems, Vol.50, No.2, pp.144-153, 2020.

[13] T.Murakami, R.Nakamura, F.Yu, and K.Ohnishi, "Force Sensorless Compliant Control Based on Reaction Force Estimation Observer in Multi-Degrees-of-Freedom Robot" Journal of RSJ, Vol. 11, No. 5, pp. 765-768, 1993.